



# Oligocene-Miocene burial and exhumation of the Southern Pyrenean foreland quantified by low-temperature thermochronology

Charlotte Fillon, Cécile Gautheron, Pieter van Der Beek

## ► To cite this version:

Charlotte Fillon, Cécile Gautheron, Pieter van Der Beek. Oligocene-Miocene burial and exhumation of the Southern Pyrenean foreland quantified by low-temperature thermochronology. *Journal of the Geological Society*, 2013, 107, pp.67 -77. 10.1144/jgs2012-051 . hal-00772598

**HAL Id: hal-00772598**

**<https://hal.science/hal-00772598>**

Submitted on 10 Jan 2013

**HAL** is a multi-disciplinary open access archive for the deposit and dissemination of scientific research documents, whether they are published or not. The documents may come from teaching and research institutions in France or abroad, or from public or private research centers.

L'archive ouverte pluridisciplinaire **HAL**, est destinée au dépôt et à la diffusion de documents scientifiques de niveau recherche, publiés ou non, émanant des établissements d'enseignement et de recherche français ou étrangers, des laboratoires publics ou privés.

**Oligocene-Miocene burial and exhumation of the Southern Pyrenean foreland  
quantified by low-temperature thermochronology**

Charlotte Fillon<sup>1\*</sup>, Cécile Gautheron<sup>2</sup> and Peter van der Beek<sup>1</sup>

1. Institut des Sciences de la Terre, Université Joseph Fourier – Grenoble I, CNRS, BP 53,  
38041 Grenoble, France

2. UMR IDES – CNRS8148, Interactions et Dynamique des Environnements de Surface,  
Université Paris Sud, 91405 Orsay, France

cecile.gautheron@u-psud.fr

pvdbeek@ujf-grenoble.fr

**\* corresponding author: charlotte.fillon@ujf-grenoble.fr**

## 15    **Abstract**

16    The central Pyrenees experienced an episode of rapid exhumation in Late Eocene-Early Oligocene  
17    times. Erosional products shed from the range during this time were deposited in large paleovalleys of  
18    the southern flank of the Axial Zone, leading to significant sediment accumulation. A recent numerical  
19    modelling study of the post-orogenic exhumation and relief history of the central Axial Zone allowed  
20    us to constrain this valley-filling episode in terms of timing and thickness of conglomeratic deposits.  
21    This paper aims to test these results for the southern fold-and-thrust belt using apatite fission-track and  
22    (U-Th)/He analysis on detrital samples from the Tremp-Graus and Ager basins. Inverse thermal-  
23    history modelling of the low-temperature thermochronology data indicates that the fold-and-thrust belt  
24    was covered during the Late-Eocene to Miocene by 0.7 to 1.6 km of sediments and confirms the  
25    timing of re-exhumation of the valleys during the Miocene. A detailed analysis of the apatite (U-Th)/He  
26    results shows that the significant scatter in grain ages can be explained by the influence of alpha-recoil  
27    damage with varying eU content together with distinct pre-depositional thermal histories; the age  
28    scatter is consistent with initial exhumation of the sediment sources during the Triassic and Early  
29    Cretaceous.

30

## 31    **1. Introduction**

32

33    The southern central Pyrenees have figured prominently in studies of orogenic wedge building,  
34    thrusting sequences and interactions between tectonics and surface processes, in part because of the  
35    exceptional exposure of syn-tectonic strata (Puigdefàbregas and Souquet 1986; Vergés and Muñoz  
36    1990) and the quality of the ECORS seismic profile (ECORS Pyrenees Team 1988) shot through this  
37    area.

38

39    Low-temperature thermochronology (mainly apatite fission-track; AFT) data (Fitzgerald *et al.* 1999;  
40    Sinclair *et al.* 2005) provide evidence for a phase of rapid exhumation of the Axial Zone of the central  
41    Pyrenees during Late Eocene – Early Oligocene times, accompanied by the development of a crustal-  
42    scale duplex (Muñoz 1992; Beaumont *et al.* 2000). The conglomeratic erosional products of this phase  
43    of rapid exhumation were hypothesized to have buried the southern flank of the Axial Zone in a late  
44    orogenic stage of its evolution, and to have been removed ~20 Myr later as post-orogenic incision of  
45    the Ebro drainage system reached the area (Coney *et al.* 1996). Recent magnetostratigraphic studies  
46    (Beamud *et al.* 2003; 2011) have confirmed the depositional ages of these conglomerates, while the  
47    link to exhumation of the Axial Zone is clearly established by their sedimentology (Vincent 2001).  
48    However, the amount, extent and timing of excavation of these conglomerates have yet to be  
49    quantified in the foreland basin where low-temperature thermochronological data are scarce. The only

currently available data are AFT ages and track-length distributions from the conglomeratic deposits themselves (Beamud *et al.* 2011; Rahl *et al.* 2011), which confirm the timing of rapid erosional unroofing of the Axial Zone and suggest that the deposits were sufficiently thick to result in partial AFT annealing in samples from their base.

Two of us have recently constrained the thickness of the conglomerate deposits and the timing of their re-incision, using thermo-kinematic modelling constrained by the existing thermochronology dataset in the Southern Axial Zone (Fillon and van der Beek 2012). These models predict a thickness of the deposits of ~2 km on the southern flank of the Axial Zone, which was reached shortly after 30 Ma. Valley incision is predicted to have occurred from Late Miocene times (9 Ma) onward, which we link to the base-level drop resulting from opening of the Ebro Basin to the Mediterranean (Garcia-Castellanos *et al.* 2003; Urgelés *et al.* 2011). We thus have proposed a scenario of topographic evolution from Axial Zone data that we extrapolated to the southern Pyrenean foreland, but no data were available to test our model predictions.

Low temperature apatite fission-track (AFT) and (U-Th)/He (AHe) thermochronology provides a powerful tool to constrain the thermal history of the foreland. The AFT and AHe thermochronometers are sensitive to the 50-120 °C and 40-110 °C temperature ranges respectively (Farley 2000; Shuster and Farley 2009), therefore their combination can be used to constrain burial and exhumation in the fold-and-thrust belt from depths between ~1.5 and 3.5 km, depending on the local geothermal gradient.

We present new AFT and AHe data from Late Cretaceous-Palaeocene “Garumnian” sandstones collected in the Tremp-Graus and Ager basins of the southern central Pyrenees (Fig. 1), in order to provide direct estimates of the thickness and extent of the overlying conglomerate deposits, as well as to further constrain the timing of excavation of the basin. The AHe thermochronometer is very sensitive and requires high-quality samples, rendering the application of this method challenging in sedimentary samples. However, we will show that despite limited and relatively scattered AHe ages, we are able to obtain consistent Mesozoic to Cenozoic exhumation histories for three samples located in the north, centre and south of the fold-and-thrust belt. We use a new thermal-history inversion code (Gallagher 2012) that allows incorporation of variable AFT-annealing and AHe-diffusion kinetics.

## **2. Tectono-sedimentary evolution of the South Central Pyrenees**

The south-central Pyrenean fold-and-thrust belt (also called South Central Unit, SCU) developed with the collision of the Iberian and European plates in the Late Cretaceous. Underthrusting of the Iberian plate below the European plate created a doubly-vergent Pyrenean wedge. The southern Pyrenees

evolved as the pro-wedge by inversion of Cretaceous extensional structures (Puigdefàbregas and Souquet 1986; Bond and McClay 1995) followed by in-sequence thrust propagation towards the south (Vergés and Muñoz 1990; Muñoz 1992; Vergés *et al.* 1995; Beaumont *et al.* 2000). The fold-and-thrust belt propagated further in the SCU, compared to the regions east and west of it, by sliding on a thick Triassic evaporite layer (Fig. 1c). Thrusting is in-sequence at first order, with activation of the Boixols thrust initiated in the Late Cretaceous, followed by the Montsec thrust, which transported the Tremp-Graus Basin in a piggy-back manner from Paleocene to Late Eocene times (Puigdefàbregas *et al.* 1992), and finally the frontal Sierras Marginales thrust sheet, active from Middle Eocene to Late Oligocene times (see Fig. 1 for locations).

From the ECORS seismic profile (ECORS Pyrenees Team 1988; Choukroune and ECORS Team 1989), as well as modelling and thermochronological studies of the Southern Axial Zone (Beaumont *et al.* 2000; Sinclair *et al.* 2005; Fitzgerald *et al.* 2006; Gibson *et al.* 2007; Metcalf *et al.* 2009), rapid exhumation of the internal units (Nogueres, Orri and Rialp, Fig. 1c) is known to have occurred by vertical stacking (Muñoz 1992; Vergés *et al.* 1995) during Middle Eocene to Early Oligocene times. Thermo-kinematic modelling of the *in-situ* low-temperature thermochronology (AFT and AHe) dataset predicts exhumation rates of  $2.8 \pm 0.3$  km Myr<sup>-1</sup> between 37 and 30 Ma in that area (Fillon and van der Beek 2012). This rapid exhumation was associated with strong erosion of the southern Axial Zone, the products of which were deposited in pre-existing palaeo-valleys as a thick pile of conglomerates currently mainly exposed in the Sis, Gorp and La Pobla massifs (Fig. 1b). These palaeo-valleys probably represented sediment transfer zones, supplying the Huesca fan system (Vincent 2001), one of the main drainage systems of the Southern Central Pyrenees (with the Luna fan system to the West) during Oligocene-Miocene times. The link between exhumation of the internal massifs and deposition of the conglomerates has been confirmed by provenance studies (Vincent 2001) and by AFT analysis of pebbles from the Sis conglomerates (Beamud *et al.* 2011; Rahl *et al.* 2011), which both reveal unroofing of the Axial Zone and deposition of its erosional products in the basin.

Present-day remnants of these extensive syn- to post-tectonic conglomerate deposits include the Senterada and La Pobla basins (Beamud *et al.* 2003; Beamud *et al.* 2011), the Sis conglomerates (Vincent, 2001), the Oliana fan (to the east of the CSU; Burbank *et al.* 1992b) and the Huesca fan (southwest of our study area; Friend *et al.* 1996); they reach a maximum thickness of ~1000 m. Magnetostratigraphic studies constrain deposition of the Sis conglomerates at ~40 to 27 Ma (Beamud *et al.* 2003; Beamud *et al.* 2011), deposition of similar conglomerates to the east of the CSU, in the Oliana area, at ~40 to 36 Ma (Burbank *et al.* 1992a), and in the Sierras Marginales thrust sheet between 36.5 and 24.7 Ma (Meigs *et al.* 1996). The period of strong exhumation/erosion/deposition was synchronous with closure of the Atlantic connection of the Ebro foreland basin at 36 Ma (Costa *et*

*al.* 2009). The basin became endorheic at that time and remained so until Late Miocene times (Arenas and Pardo 1999; Garcia-Castellanos *et al.* 2003; Arche *et al.* 2010; Urgelés *et al.* 2011). During its endorheic phase, the basin was progressively filled by conglomeratic deposits at its borders, grading to lacustrine sediments in its centre, and developed into a large overfilled foreland basin.

### **3. Mesozoic pre-depositional history**

Recently, two independent studies have reported zircon fission-track (ZFT), U-Pb and (U-Th)/He (ZHe) ages of samples from the SCU (Filleaudeau *et al.* 2011; Whitchurch *et al.* 2011). ZHe analysis of Garumnian sandstones of the Tresp Basin (sample ORC2; Filleaudeau *et al.* 2011) shows three main age populations (Triassic, Early Cretaceous and Late Cretaceous), interpreted to reflect distinct Mesozoic exhumation events affecting the source area(s). Whitchurch *et al.* (2011) applied detrital ZFT dating to Garumnian sandstones of the Ager basin and found the same Early and Late Cretaceous exhumation events, together with Carboniferous (Variscan) ZFT ages. A sample collected from the Aren formation (the stratigraphic unit just below the Garumnian in the Tresp Basin) presents Early Cretaceous and Carboniferous ZFT age peaks, lacking Late Cretaceous ages. The combination of these two datasets shows an important phase of Early Cretaceous source-area exhumation at  $134 \pm 15$  Ma (all uncertainties combined), with less well expressed events at  $\sim 80$  Ma,  $\sim 225$  Ma and 300-330 Ma. We will discuss later the imprint of these pre-depositional exhumation phases on our sample ages.

### **4. Low-temperature thermochronology**

Five samples (AN01 to AN05) were collected along a N-S profile in Garumnian facies sandstones. These continental deposits of Maastrichtian-Middle Palaeocene (65-60 Ma) age crop out extensively throughout the fold-and-thrust belt (Fig. 1b). Other lithologies were also sampled, including Eocene sandstones, Santonian turbidites and volcanic rocks of the Noguères zone, but none of these provided sufficient high-quality apatite grains for thermochronological analysis.

#### **4.1. Apatite Fission-Track thermochronology**

Samples were prepared and analyzed at ISTERre (Grenoble, France). Apatite grains were separated from fine- to medium-grained sandstone samples using standard heavy-liquid and magnetic separation techniques. Apatite aliquots were mounted in epoxy, polished to expose internal crystal surfaces, and etched with 5.5 M HNO<sub>3</sub> for 20 s at 21 °C. Low-U muscovite sheets were fixed to the mounts, to be used as external detectors, and samples were irradiated in the FRM II Research Reactor at the Technische Universität München (Germany). Apatite samples were irradiated together with IRMM 540R dosimeter glasses and Durango and Fish Canyon Tuff age standards. After irradiation, the mica

detectors of all samples and standards were etched for 18 minutes at 21 °C in 48% HF. The samples and standards were counted dry at 1250× magnification, using an Olympus BH2 optical microscope and the FTStage 4.04 system of Dumitru (1993). Due to the low yield of apatite grains, all datable grains were counted for each sample. Fission-track ages were calculated using the zeta-calibration method and the standard fission-track age equation (Hurford and Green 1983). The  $\chi^2$ -test and age dispersion (Galbraith and Green 1990; Galbraith and Laslett 1993) were used to assess the homogeneity of AFT ages. We were able to measure horizontal confined track lengths and the lengths of the track etch pits that outcrop on the etched internal surface ( $D_{\text{par}}$ ) in four samples.

#### 4.2. Apatite (U-Th)/He analysis

Apatite grains were carefully selected according to their morphology at ISTerre. Each grain was placed into a platinum basket for He-extraction at Paris-sud University (Orsay, France). Two to five replicates were analyzed per sample. The platinum baskets were heated using a diode laser to  $1030 \pm 50$  °C during 5 minutes, allowing total He degassing; a reheat under the same conditions allowed checking for the presence of He trapped in small inclusions. The  $^4\text{He}$  content was determined by comparison with a  $1.2 \times 10^{-7}$  ccSTP  $^3\text{He}$  spike. After He extraction, platinum baskets were placed into single-use polypropylene vials. Apatite grains were dissolved one hour at 90 °C in a 50  $\mu\text{l}$   $\text{HNO}_3$  solution containing a known concentration of  $^{235}\text{U}$  and  $^{230}\text{Th}$ , and then filled with 1 ml of ultrapure MQ water. U and Th measurements followed a procedure similar to Evans *et al.* (2005). The final solution was measured for U and Th concentrations by quadrupole ICP-MS (series<sup>II</sup> CCT Thermo-Electron at LSCE, Gif-sur-Yvette, France). Analytical accuracy and reproducibility for U-Th isotope measurements by using ICP-QMS were better than  $\pm 0.5\%$  at  $2\sigma$  (Douville *et al.* 2010). The analysis was calibrated using internal and external age standards, including Limberg Tuff, Durango and FOR3, which provided mean AHe ages of  $16.8 \pm 0.7$  Ma,  $31.8 \pm 0.5$  Ma, and  $110.7 \pm 7.0$  Ma respectively. These values are in agreement with literature data, i.e.  $16.8 \pm 1.1$  Ma for the Limberg Tuff (Kraml *et al.* 2006),  $31.02 \pm 0.22$  Ma for Durango (McDowell *et al.* 2005) and  $112 \pm 10$  Ma for the internal FOR3 standard. Individual ages were corrected by each grain's ejection factor  $F_T$ , determined using the Monte Carlo simulation technique of Ketcham *et al.* (2011); the equivalent-sphere radius has been calculated using the procedure of Gautheron and Tassan-Got (2010). The  $1\sigma$  error on AHe age should be considered at 8%, reflecting the sum of errors in the ejection-factor correction and age dispersion of the standards.

## 5. Results

Apatite fission tracks were counted and measured in 4 samples located in the north (AN04), centre (AN03, AN02) and south (AN01) of the fold-and-thrust belt (see Fig. 1 for location); the results are reported in Fig. 2 and Table 1. Only sample AN01, collected south of the Montsec thrust (Fig. 1),

close to the Ager basin sample of (2011), shows a single age component ( $144 \pm 11$  Ma). The other samples, for which more grains were counted, fail the  $\chi^2$ -test and have age dispersions  $>20\%$ , with central ages between  $64 \pm 5$  and  $77 \pm 6$  Ma. Individual samples contained insufficient dated grains to deconvolve the sample ages into age components. However, since the samples were collected in the same stratigraphic unit and show similar age structures, we calculated age components from the combined data, using the radial-plotter software of Vermeesch (2009). Three age peaks are found when pooling all single-grain ages: the major age component is Late Cretaceous in age ( $76.1 \pm 3.7$  Ma), the second peak age is Late Paleocene (i.e., younger than the depositional age;  $51.7 \pm 3.2$  Ma), and a minor Early Cretaceous peak age is found at  $142 \pm 10$  Ma, with Early Cretaceous single-grain ages encountered in all samples (Fig.2).

The youngest age population is clearly younger than the depositional age and single-grain ages  $<60$  Ma are found in all samples except AN01, suggesting that they have been partially reset by post-depositional burial. Mean track lengths (MTL) are very short, ranging from  $10.1 \mu\text{m}$  in AN01 to  $12.2 \mu\text{m}$  in AN03 with standard deviations between  $1.0$  and  $2.2 \mu\text{m}$ , indicating relatively slow long-term exhumation rates. Note, however, that only between 10 and 27 track lengths could be measured in these samples due to the low apatite yield.

Apatite (U-Th)/He analyses were also performed on four samples: AN01, 02, 03 and AN05 (Fig. 3, Table 2). A striking feature of the AHe ages is their large scatter; single-grain ages vary from 3.9 to 169 Ma. There appears to be some correlation between AHe ages and the effective uranium content ( $eU = [U] + 0.24 \times [Th]$ , expressed in ppm) of the grains, which varies between 4 and 25 ppm in samples AN01, 02 and 03 (Fig. 3a). The relationship between single-grain AHe ages and eU content reflects the increase of closure temperature as a function of the amount of  $\alpha$ -recoil damage, for which eU content is a convenient proxy (Shuster *et al.* 2006; Shuster and Farley 2009). Moreover, the rapidly increasing ages for  $eU > 15$  ppm, with less variation below this value (Fig. 3a), are consistent with a model in which He-retention increases non-linearly with the amount of  $\alpha$ -recoil damage (Shuster *et al.*, 2006; Flowers *et al.* 2009). Only sample AN05 does not fit this correlation; we suspect that this may be related to its very high eU content and, in particular, quite extreme Th concentration compared to the other samples. Thus, the AHe ages cannot be interpreted directly, but the Late Miocene-Pliocene ages measured in samples AN01, AN02 and AN03 imply post-depositional burial and exhumation of the basin. We will test the timing and amount of burial / exhumation through numerical inversion of the data in the next section.



## 6. Thermal-history modelling

In order to test what constraints the data provide on the post-depositional thermal history of the samples, we use an inversion model (Gallagher *et al.* 2009, Gallagher 2012) that allows extracting both optimal thermal histories and AFT annealing/AHe diffusion parameters by a Markov chain Monte Carlo (MCMC) sampling method. The inversion code incorporates recent kinetic models of He diffusion proposed by Flowers *et al.* (2009) and Gautheron *et al.* (2009), as well as the most recent multi-kinetic AFT annealing model of Ketcham *et al.* (2007). The modelling proceeds from an initial randomly chosen time-temperature path and set of kinetic parameters, for which a probability that the model fits the data is calculated. Then the parameters are slightly perturbed, the probability of fitting the data is recalculated and compared to the initial model. The model with the highest probability is retained. This procedure is repeated a large number of times (the number of iterations being chosen by the user), providing a large collection of models with their associated probabilities that allow calculating model statistics (probability distributions of model parameters, etc.). A full explanation of the modelling procedure is provided in Gallagher (2012).

### 6.1. Model set-up

The parameter space (time,  $t$  and temperature,  $T$ ) has been subdivided into three  $T$ - $t$  boxes: from 300 Ma (beginning of the model run) to 70 Ma with temperatures between 140 °C and 0 °C, from 70 to 60 Ma with a temperature of  $10 \pm 10$  °C (e.g. surface conditions), and finally from 60 Ma to present, with a temperature range of 140 °C to 0 °C. By doing this, the only constraint we impose on the model is the deposition time. The results are the product of 200,000 iterations, which is a sufficient amount to obtain a stable and robust solution (see discussion in Gallagher 2012). We present results of inversions for samples AN01, 02 and 03, which were analysed with both AFT and AHe thermochronology; samples AN04 and AN05, which come from the same structural position but for which only AFT (AN04) or AHe (AN05) measurements were available, were combined for a test model but do not provide sufficient thermal constraints to obtain a well-defined  $T$ - $t$  path.

As we use a multikinetic AFT annealing algorithm (Ketcham *et al.* 2007) in this study, the single grain-age counting data and track-length measurements were incorporated in the model and combined with the average  $D_{\text{par}}$  (i.e. we do not take potential intra-sample kinetic variation into account). We acknowledge that the number of track lengths measured in the samples is less than optimal for inverse thermal history modelling; however, this limitation is offset by the fact that we have both AFT and AHe data and exploit variable annealing and diffusion kinetics.

The He-diffusion models of Gautheron *et al.* (2009) and Flowers *et al.* (2009) were used to reproduce He-diffusion behaviour in apatite. These two models include the influence of  $\alpha$ -recoil damage and its

annealing on He-diffusion kinetics; in particular, they predict He retentivity to increase either linearly (Gautheron *et al.* 2009) or non-linearly (Flowers *et al.* 2009) with the amount of  $\alpha$ -recoil damage. Predicted AHe ages by the two models mainly differ for low eU contents (15-25 ppm), because this is the range where the amount of  $\alpha$ -recoil damage corresponds to the slope change in the diffusion law defined by natural and experimental data (Shuster *et al.* 2006; Shuster and Farley 2009). The simulations therefore predict slightly different thermal histories depending on which He-diffusion model is used; we will only present models using the Flowers *et al.* (2009) diffusion algorithm here; modelling results obtained using the Gautheron *et al.* (2009) diffusion algorithm are presented in Supplementary Figure 1.

The inversion procedure used here implicitly assumes that all grains share a single pre-depositional thermal history, whereas the zircon data discussed in Section 3 show that these sediments were derived from multiple sources with different pre-depositional histories. We will assess the effect of this simplification in the discussion (Section 7.2).

## 6.2. Inferred thermal histories

The models predict very similar  $T$ - $t$  paths for all three samples (Fig. 4), in accordance with their similar stratigraphic and structural position, showing burial from their time of deposition until Miocene-Pliocene times, followed by exhumation until the present-day. The pre-deposition  $T$ - $t$  path is poorly constrained for samples AN01 and AN02, in contrast to the model for sample AN03, which predicts a well-constrained pre-depositional history with linear cooling from the Early Cretaceous (130 °C at 100 Ma) to the time of Garumnian sandstone deposition. For this sample, the model predicts burial to a temperature of ~70 °C reached between 11 and 5 Ma, before final exhumation.

Sample AN01 produced the widest range of single-grain AHe ages (7 Ma and 77 Ma); although the AFT age (144±11 Ma) suggests a single source age. The sample is also furthest from the preserved conglomeratic massifs. Nevertheless, the model predicts significant burial, to a maximum temperature of 80 °C, and an onset of Miocene exhumation between 20 and 10 Ma. The  $T$ - $t$  path of sample AN02 is quite similar, although this sample appears to have been buried most deeply, reaching a temperature of up to 95 °C. The predicted onset of final exhumation is well constrained at 7 Ma. Finally, we observe that the maximum Cenozoic burial temperatures predicted by the models are consistent with their corresponding AFT ages; maximum predicted burial temperatures are higher for samples with younger central AFT ages.

## 7. Discussion

### 7.1. Sensitivity to eU variations

To test the thermal histories provided by inverse modelling and the match with our AHe ages, the “expected” thermal histories (i.e. the weighted-average  $T-t$  path for the probability distributions shown in Fig. 4; cf. Gallagher 2012) for the three samples have been introduced in a forward model (Ketcham *et al.* 2005) to predict AHe ages for a grain size equal to the average size of our analysed crystals (equivalent-sphere radius of 57  $\mu\text{m}$ ) and eU contents varying from 5 to 30 ppm, using the He-diffusion model of Flowers *et al.* (2009). A comparison of predicted ages with our AHe data (Fig. 5) shows that both single-grain ages of sample AN02, as well as most single-grain ages of sample AN03 are in good agreement with the modelled path. Therefore, this test shows that the age scatter of these samples can be largely explained by their varying eU content. Conversely, some grains of samples AN01 and AN03 do not fit the modelled relationship between age and eU; therefore the measured ages could have been influenced by another parameter, such as a different pre-depositional history. We will test that possibility in the following section.

### 7.2. Influence of the pre-depositional history

The inverse modelling procedure we used cannot take into account variable pre-depositional histories of these detrital grains. However, the detrital ZFT and ZHe data of Whitchurch *et al.* (2011) and Filleaudeau *et al.* (2012) provide evidence for variability in timing and rates of source-area exhumation, as discussed in Section 3. We thus test to what degree such variable pre-depositional exhumation histories could explain the encountered dispersion of AHe ages.

The ZFT and ZHe data presented in Section 3 show pre-depositional exhumation ages between  $\sim 80$  and  $\sim 300$  Ma. From this starting point, we tested the influence of the pre-depositional history and eU content by performing forward modelling (Ketcham 2005), using the AFT annealing model of Ketcham *et al.* (2007) and the AHe-diffusion model of Flowers *et al.* (2009), with the same parameter values as in Section 7.1. We imposed the post-depositional scenario from the inversion results presented previously and tested how the final AHe age varies as a function of eU, maximum post-depositional temperature ( $T_{\text{max}}$ ) and onset time of initial (pre-depositional) exhumation (Fig. 6a). The results are presented as contours of predicted AHe ages as a function of eU and onset time in Fig. 6b and 6c, for  $T_{\text{max}}$  of 70 and 80  $^{\circ}\text{C}$  respectively.

This forward modelling differs from the inverse modelling presented previously in two important aspects, therefore inducing somewhat different results: first, the forward models use fixed values for the diffusion parameters, whereas the inverse models allow varying these within the uncertainties

propagated from the original experiments (Gallagher 2012). Second, we fix  $T_{\max}$  as well as its timing and the overall shape of the thermal history path in the forward models, whereas these have more degrees of freedom in the inversions and show, for instance, clear tradeoffs between  $T_{\max}$  and timing of initial (pre-depositional) cooling. We use these forward models to illustrate the effects of variable  $T_{\max}$ , eU and pre-depositional history on the measured AHe ages rather than to provide additional constraints on these parameters.

For the two burial temperatures tested, the modelling reveals the same patterns, in agreement with the relationship we expect between AHe age, eU content and  $T_{\max}$ . The modelled ages are older when initial exhumation starts earlier and for higher eU contents. The predicted ages are younger when  $T_{\max}$  increases; the maximum modelled AHe ages are 155 and 120 Ma for  $T_{\max}$  of 70 and 80 °C, respectively. Moreover, for the same eU, the age scatter decreases with increasing  $T_{\max}$ . For example, for an eU of 16 ppm (the average eU value of our grains), modelled ages vary from 10 to 105 Ma as a function of onset time of initial exhumation for  $T_{\max} = 70$  °C, but only from 10 to 40 Ma for  $T_{\max} = 80$  °C.

These forward models confirm the hypothesis that the pre-depositional history of the detrital grains can have a major effect on AHe age variations. With these results, we can also identify what variability in timing of pre-depositional exhumation would be required to explain the scatter in our AHe ages, by plotting the ages and eU values of our samples on the contour plots (Fig.7b). First of all, we note that the forward model with  $T_{\max} = 70$  °C provides the best fit to the combined data; this value is within the range of predictions of all inverse models. Secondly, when looking at the  $T_{\max} = 70$  °C plot, we can conclude that all grains except AN011 fit with a pre-depositional exhumation phase starting between 150 and 90 Ma, which is in good agreement with the ZHe and ZFT age distributions of Filleaudeau et al. (2012) and Whitchurch *et al.* (2011), which record a major Early Cretaceous (~120-150 Ma) exhumation phase and a less well-expressed phase in the Late Cretaceous (~80 Ma). These results are also in agreement with the expected model from the thermal-history inversion of AN02 and AN03, predicting an onset of initial exhumation before the Late-Cretaceous (i.e. >100 Ma). Only the age of AN011 is outside of this range and suggests Triassic initial cooling, consistent with the occurrence of Triassic ZHe ages, which may result from a major volcanic episode associated with the emplacement of the Central Atlantic Magmatic Province (Marzoli *et al.* 1999). Our previous observations showed that the age dispersion between the two grains of this sample could not be explained by their respective eU contents alone. We thus propose that variable pre-depositional exhumation histories, with at least one grain recording Triassic initial cooling, constitute another factor to explain the variable AHe grain ages.

To conclude, our forward modelling shows that the pre-depositional history of a detrital sample can considerably influence the measured AHe ages as well as the inferred temperature of burial. In our case, it seems that a combination of variable eU and variable timing of initial exhumation, consistent with higher-temperature detrital ZHe and ZFT data, can explain the scatter in AHe ages. Moreover, the forward models suggest that most apatite grains record an Early Cretaceous pre-depositional exhumation phase.

### 7.3. Cenozoic Burial and exhumation scenario

The inverse modelling results provide values for the amount and timing of Cenozoic burial heating that range from 70 to 95 °C, with final exhumation starting between 20 and 5 Ma. Even though the modelling predicts a variable range of maximum burial temperatures and associated timing, the first-order pattern of the  $T-t$  paths in all cases shows significant burial during post-Eocene times, with subsequent exhumation starting in the Late Miocene–Early Pliocene.

We interpret the burial recorded by the samples as being due to deposition of the Late Eocene–Oligocene conglomerates produced by rapid erosion of the Axial Zone, and explain the subsequent exhumation by excavation of the modern southern Pyrenean river valleys. In this scenario, we do not take into account any tectonic activity that could be responsible for late-stage exhumation of the SCU (*i.e.*, during Miocene times). The main reason for this choice is that there is no clear evidence for such tectonic activity in the SCU, mainly because no Miocene sediments are exposed in that area. Moreover, as shown in Fig. 7, our AFT and AHe ages and the corresponding burial estimates predicted by the thermal modelling are homogeneous for all samples, despite their provenance from different thrust sheets. A few very young (Middle Miocene) AFT and AHe ages were reported further west, in the Bielsa massif (Jolivet *et al.* 2007) and to the north of the study area in the Barruera massif (Gibson *et al.* 2007), which have been interpreted as recording Miocene out-of-sequence thrusting. However, it is unclear how these results could be extrapolated to the SCU.

Estimating the thickness of the conglomerate cover requires knowledge of the local geothermal gradient. A previous interpretation of AFT data from the SCU (Beamud *et al.* 2011) used a geothermal gradient of 30 °C km<sup>-1</sup>, as constrained by numerical modelling (Zeyen and Fernández 1994) supposing a value for the thermal conductivity of sediments of 2.5 W m<sup>-1</sup> K<sup>-1</sup>. According to Fernández *et al.* (1998), however, the average present-day geothermal gradient for the SCU is 22±4 °C km<sup>-1</sup>, significantly lower than the value for the Pyrenean Axial Zone (~33 °C km<sup>-1</sup>); this discrepancy is apparently due to the high thermal conductivity (2.47 to 3.22 W m<sup>-1</sup> K<sup>-1</sup>) measured in the sediments. As there is no consensus on the subject, we will use in the following a 30 °C km<sup>-1</sup> geothermal gradient to estimate the sediment thicknesses, thus providing a conservative estimate of the amount of burial.

Using this value for the geothermal gradient and a surface temperature of 20 °C, the minimum amount of burial required to reach the  $T_{\text{max}}$  recorded by our Garumnian samples can be estimated at 2.3 km for sample AN03, 2.6 km for sample AN01 and to 3.2 km for sample AN02, with final exhumation rates of 0.13 to 0.5 km Myr<sup>-1</sup>. As the thickness of the Palaeocene-Middle Eocene sediments deposited in the Tremp-Graus Basin ranges from 1.2 km in the Montsec footwall area (sample AN01) to 1.6 km in the Tremp area (samples AN02 and AN03), our results imply a minimum thickness of post-Middle Eocene sediments of 700 m for sample AN03, 1.6 km for the sample AN02 and 1.4 km for sample AN01, as represented in Fig. 7. Note that, because the Late Eocene-Oligocene conglomerates are discordant on the Middle-Eocene and older sediments, it is difficult to estimate the exact thickness of the latter. Note also that for a lower geothermal gradient of 22 °C km<sup>-1</sup> (see paragraph above), inferred burial depths are significantly higher and require 1.6, 2.4 and 2.7 km of post-Middle Eocene sediments, respectively, for samples AN03, AN01 and AN02.

Thermo-kinematic modelling of the *in-situ* AFT and AHe dataset in the Axial Zone of the central Pyrenees (Fillon and van der Beek 2012) suggested that ~2 km of conglomeratic deposits once covered the southern flank of the central Axial Zone. The model also predicted re-incision and erosion of the conglomerates during the Tortonian (9.2±0.5 Ma), implying late-stage exhumation rates of ~0.3 km Myr<sup>-1</sup> in the valley bottoms. The AHe ages confirm this interpretation and show continuous excavation of the basin from the Late Miocene-Pliocene to the present.

Finally, it is interesting to note that our inverse models do not reproduce an Eocene signal of exhumation linked to tectonic activity of the fold-and-thrust belt. However, the Late Eocene conglomerates rest unconformably on the earlier syn-tectonic sediments, implying an initial period of burial and unroofing between the Late Cretaceous and Late Eocene. We tested for this by forcing the thermal history models to reach near-surface temperatures in the Eocene but found that this did not affect the models to any significant extent. Therefore, if there was exhumation in the Eocene it could not have been very large (>1 km) otherwise the AFT and AHe systems would have recorded this event. Our modelling results thus support the idea of a strongly overfilled Ebro basin in the Oligocene-Miocene, characterised by up to 1.6 km of sediment aggradation at its northern edge.

#### **7.4. Extent of late orogenic conglomerate deposits**

The inferred amounts of burial are consistent with what we expected for samples AN02 and AN03, as these were collected close to the remnant conglomeratic massifs and the Axial Zone. A more surprising result is obtained for sample AN01, which is located in another structural unit, south of the Montsec thrust, and quite far from the Axial Zone. The closest conglomeratic outcrops to this sample are located further east and have been dated by magnetostratigraphy at 40 to 36 Ma (Olina conglomerates; Burbank *et al.* 1992a). Nevertheless, the inversion results for sample AN01 suggest

2.6 km of burial before an onset of final exhumation between 10 and 20 Ma. These values are comparable to those obtained for the northern samples. Thus, the Ager Basin, south of the Montsec thrust (Fig. 1), seems to record the same post-Eocene burial/exhumation history as the Trespín Basin, implying that infilling by the Huesca fan sediments extended to that basin. The burial of the Ager Basin, which is not drawn in most paleo-geographic reconstructions (see Jones 2004 for example), could result from an extension of the Huesca fan further to the east, or from extension of the Oliana fan towards the west.

## 8. Conclusions

We have succeeded in modelling our dataset of AFT and AHe ages of detrital apatites to obtain consistent  $T-t$  paths using He-diffusion kinetics that are a function of radiation damage and its annealing. Our models show that the significant AHe-age scatter can be explained by variable eU content together with variable pre-depositional exhumation histories, consistent with inferences from published higher-temperature ZFT and ZHe data. Modelling of three samples predicts burial from the Late-Cretaceous to the Miocene-Pliocene to reach maximum temperatures of 70 to 95 °C, requiring at least 0.7 to 1.6 km of Late Eocene-Oligocene overburden. The inferred timing for the onset of exhumation ranges from 20 to 5 Ma, with exhumation rates of 0.13 to 0.5 km Myr<sup>-1</sup>. These modelling results thus show similar post-orogenic burial and exhumation in the southern Pyrenean foreland as previously inferred for the southern Axial Zone and suggest a Late Miocene (pre-Messinian) onset of Ebro Basin incision. They confirm that several km of sediments covered the southern Pyrenean flank and filled the Ebro Basin, consequently to the onset of endorheism in the basin.

## Acknowledgements:

This study was supported by INSU-CNRS through the European Science Foundation Topo-Europe programme “Spatial and temporal coupling between tectonics and surface processes during lithosphere inversion of the Pyrenean-Cantabrian mountain belt (PyrTec)”. It forms part of CF's PhD project at Université Joseph Fourier, supported by the French Ministry for Research and Higher Education. Vincent Bouvier, Rosella Pinna and Louise Bordier are thanked for AFT sample preparation, U-Th chemistry and help during ICP-MS measurement at LSCE (Gif sur Yvette), respectively. Eric Douville is thanked for providing access to the ICP-MS. AHe age measurements at Orsay were funded by the ANR-06-JCJC-0079 project granted to C. Gautheron. The fission-track lab at ISTERRE is supported by Université Joseph Fourier and INSU-CNRS. We thank Kerry Gallagher for providing a pre-publication version of the QTQt thermal-history inversion code and for advise in running it. Constructive reviews by Hugh Sinclair and an anonymous reviewer, as well as comments by editor Andy Carter, significantly improved the manuscript.

## References

- Arche, A., G. Evans and E. Clavell (2010). "Some considerations on the initiation of the present SE Ebro river drainage system: Post- or pre-Messinian?" *Journal of Iberian Geology* **36**(1): 73-85.
- Arenas, C. and G. Pardo (1999). "Latest Oligocene-Late Miocene lacustrine systems of the north-central part of the Ebro Basin (Spain): sedimentary facies model and palaeogeographic synthesis." *Palaeogeography, Palaeoclimatology, Palaeoecology* **151**(1-3): 127-148.
- Beamud, E., M. Garcés, L. Cabrera, J. A. Muñoz and Y. Almar (2003). "A middle to late Eocene continental chronostratigraphy from NE Spain." *Earth and Planetary Science Letters* **216**: 501-504.
- Beamud, E., J. A. Muñoz, P. G. Fitzgerald, S. L. Baldwin, M. Garcés, L. Cabrera and J. R. Metcalf (2011). "Magnetostratigraphy and detrital apatite fission track thermochronology in syntectonic conglomerates: constraints on the exhumation of the South-Central Pyrenees." *Basin Research* **23**(3): 309-331.
- Beaumont, C., J. A. Muñoz, J. Hamilton and P. Fullsack (2000). "Factors controlling the Alpine evolution of the central Pyrenees inferred from a comparison of observations and geodynamical models." *Journal of Geophysical Research* **105**: 8121-8145.
- Bond, R. and K. McClay (1995). Inversion of a Lower Cretaceous extensional basin, south central Pyrenees, Spain. *Basin Inversion*. J. Buchanan, P., Geological Society of London Special Publications. **88**: 415-431.
- Burbank, D. W., C. Puigdefàbregas and J. A. Muñoz (1992a). "The chronology of the Eocene tectonic and stratigraphic development of the eastern Pyrenean foreland basin, northeast Spain." *Geological Society of America Bulletin* **104**: 1101-1120.
- Burbank, D. W., J. Vergés, J. A. Muñoz and P. Benthams (1992b). "Coeval hindward- and forward-imbricating thrusting in the south-central Pyrenees, Spain: Timing and rates of shortening and deposition." *Geological Society of America Bulletin* **104**: 3-17.
- Choukroune, P. and ECORS Team (1989). "The ECORS Pyrenean deep seismic profile reflection data and the overall structure of an orogenic belt." *Tectonics* **8**: 23-39.
- Coney, P. J., J. A. Muñoz, K. R. McClay and C. A. Evnechick (1996). "Syntectonic burial and post-tectonic exhumation of the southern Pyrenees foreland fold-thrust belt." *Journal of the Geological Society, London* **153**(1): 9-16.
- Costa, E., M. Garcés, M. López-Blanco, E. Beamud, M. Gómez-Paccard and J. Cruz Larrasoña (2009). "Closing and continentalization of the South Pyrenean foreland basin (NE Spain): magnetochronological constrains." *Basin Research* **22**(6): 904-917.
- Douville, E., E. Sallé, N. Frank, M. Eisele, E. Pons-Branchu and S. Ayrault (2010). "Rapid and accurate U-Th dating of ancient carbonates using inductively coupled plasma-quadrupole mass spectrometry." *chemical geology* **272**(1-4): 1-11.
- Dumitru, T. A. (1993). "A new computer-automated microscope stage system for fission-track analysis." *Nuclear Tracks and Radiation Measurements* **21**(4): 575-580.



- ECORS Pyrenees Team (1988). "The ECORS deep seismic profile reflection survey across the Pyrenees." *Nature* **331**: 508-811.
- Evans, N. J., J. P. Byrne, J. T. Keegan and L. E. Dotter (2005). "Determination of uranium and thorium in zircon, apatite, and fluorite: Application to laser (U-Th)/He thermochronology." *Journal of Analytical Chemistry* **60**(12): 1300-1307.
- Farley, K. A. (2000). "Helium diffusion from apatite: general behavior as illustrated by Durango fluorapatite." *J. Geophys. Res.*(105): 2903–2914.
- Fernández, M., I. Marzan, A. Correia and E. Ramalho (1998). "Heat flow, heat production, and lithospheric thermal regime in the Iberian Peninsula." *Tectonophysics* **291**(1-4): 29-53.
- Filleaudeau, P. Y., F. Mouthereau and R. Pik (2012). "Thermo-tectonic evolution of the south-central Pyrenees from rifting to orogeny: insights from detrital zircon U/Pb and (U-Th)/He thermochronometry " *Basin Research* **24**(4): 401-417.
- Fillon, C. and P. van der Beek (2012). "Post-orogenic evolution of the southern Pyrenees: constraints from inverse thermo-kinematic modelling of low-temperature thermochronology data." *Basin Research* **24**(4): 418-436.
- Fitzgerald, P. G., S. L. Baldwin, L. E. Webb and P. B. O'Sullivan (2006). "Interpretation of (U-Th)/He single grain ages from slowly cooled crustal terranes: A case study from the Transantarctic Mountains of southern Victoria Land." *Chemical Geology* **225**(1-2): 91-120.
- Fitzgerald, P. G., J. A. Muñoz, P. J. Coney and S. L. Baldwin (1999). "Asymmetric exhumation across the Pyrenean orogen: implications for the tectonic evolution of a collisional orogen." *Earth and Planetary Science Letters* **173**: 157-170.
- Flowers, R. M., R. A. Ketcham, D. L. Shuster and K. A. Farley (2009). "Apatite (U-Th)/He thermochronometry using a radiation damage accumulation and annealing model." *Geochimica et Cosmochimica Acta* **73**(8): 2347-2365.
- Friend, P. F., M. J. Lloyd, R. McElroy, J. Turner, A. Van Gelder and S. J. Vincent (1996). Evolution of the central part of the northern Ebro basin margin, as indicated by its Tertiary fluvial sedimentary infill. *Tertiary Basins of Spain*. P.F. Friend, C. J. Dabrio (eds.), Cambridge University press: 166-172.
- Galbraith, R. F. and P. F. Green (1990). "Estimating the component ages in a finite mixture." *Nuclear Tracks and Radiation Measurements* **17**(3): 197-206.
- Galbraith, R. F. and G. M. Laslett (1993). "Statistical models for mixed fission track ages." *Nuclear Tracks and Radiation Measurements* **21**(4): 459-470.
- Gallagher, K. (2012). "Transdimensional inverse thermal history modeling for quantitative thermochronology." *Journal of Geophysical Research* **117**(B2): B02408, doi: 10.1029/2011jb008825.
- Gallagher, K., K. Charvin, S. Nielsen, M. Sambridge and J. Stephenson (2009). "Markov chain Monte Carlo (MCMC) sampling methods to determine optimal models, model resolution and model choice for Earth Science problems." *Marine and Petroleum Geology* **26**(4): 525-535.
- Garcia-Castellanos, D., J. Vergés, J. Gaspar-Escribano and S. Cloetingh (2003). "Interplay between tectonics, climate, and fluvial transport during the Cenozoic evolution of the Ebro Basin (NE Iberia)." *Journal of Geophysical Research* **108**(B7): 2347, doi: 10.1029/2002JB002073.

- Gautheron, C. and L. Tassan-Got (2010). "A Monte Carlo approach of diffusion applied to noble gas/helium thermochronology." *Chemical Geology* **273**: 212-224.
- Gautheron, C., L. Tassan-Got, J. Barbarand and M. Pagel (2009). "Effect of alpha-damage annealing on apatite (U-Th)/He thermochronology." *Chemical Geology* **266**(3-4): 157-170.
- Gibson, M., H. D. Sinclair, G. J. Lynn and F. M. Stuart (2007). "Late- to post-orogenic exhumation of the Central Pyrenees revealed through combined thermochronological data and modelling." *Basin Research* **19**(3): 323-334.
- Hurford, A. J. and P. F. Green (1983). "The zeta age calibration of fission-track dating." *Chemical Geology* **41**: 285-317.
- ICC (2002). Mapa geològic de Catalunya 1:250 000. Institut Cartogràfic de Catalunya.
- Jolivet, M., P. Labaume, P. Monié, M. Brunel, N. Arnaud and M. Campani (2007). "Thermochronology constraints for the propagation sequence of the south Pyrenean basement thrust system (France-Spain)." *Tectonics* **26**: TC5007, doi: 10.1029/2006TC002080.
- Jones, S. J. (2004). "Tectonic controls on drainage evolution and development of terminal alluvial fans, southern Pyrenees, Spain." *Terra Nova* **16**(3): 121-127.
- Ketcham, R. A. (2005). Forward and reverse modeling of low-temperature thermochronology data. *Low-Temperature Thermochronology: Techniques, Interpretations and Applications*. P. W. Reiners, T. A. Ehlers (eds.), Rev. Mineral. Geochem. **58**: 275-314.
- Ketcham, R. A., A. Carter, R. A. Donelick, J. Barbarand and A. J. Hurford (2007). "Improved modeling of fission-track annealing in apatite." *American Mineralogist* **92**: 789-798.
- Ketcham, R. A., C. Gautheron and L. Tassan-Got (2011). "Accounting for long alpha-particle stopping distances in (U-Th-Sm)/He geochronology: Refinement of the baseline case." *Geochimica et Cosmochimica Acta* **75**: 7779-7791.
- Kraml, M., R. Pik, M. Rahn, R. Selbekk, J. Carignan and J. Keller (2006). "A new multi-mineral age reference material for  $^{40}\text{Ar}/^{39}\text{Ar}$ , (U-Th)/He and fission track dating methods: The Limberg t3 tuff." *Geostandards and Geoanalytical Research* **30**(2): 73-86.
- Marzoli, A., P. R. Renne, E. M. Picirillo, G. Bellieni and A. De Min (1999). "Extensive 200-million-year-old continental flood basalts of the central Atlantic magmatic province." *Science* **284**: 616-618.
- McDowell, F. W., W. C. McIntosh and K. A. Farley (2005). "A precise  $^{40}\text{Ar}/^{39}\text{Ar}$  reference age for the Durango apatite (U-Th)/He and fission-track dating standard." *Chemical Geology* **214**(3-4): 249-263.
- Meigs, A. J., J. Verges and D. W. Burbank (1996). "Ten-million-year history of a thrust sheet." *Geological Society of America Bulletin* **108**(12): 1608-1625.
- Metcalf, J. R., P. G. Fitzgerald, S. L. Baldwin and J. A. Muñoz (2009). "Thermochronology of a convergent orogen: Constraints on the timing of thrust faulting and subsequent exhumation of the Maladeta Pluton in the Central Pyrenean Axial Zone." *Earth and Planetary Science Letters* **287**(3-4): 488-503.

- Muñoz, J. A. (1992). Evolution of a continental collision belt: ECORS Pyrenees crustal balanced cross section. *Thrust Tectonics*. K. R. McClay (ed.). London, Chapman & Hall: 235-246.
- Puigdefàbregas, C., J. A. Muñoz and J. Vergés (1992). Thrusting and foreland basin evolution in the southern Pyrenees. *Thrust Tectonics*. K. R. McClay (ed.). London, Chapman & Hall: 247-254.
- Puigdefàbregas, C. and P. Souquet (1986). "Tecto-sedimentary cycles and depositional sequences of the Mesozoic and Tertiary from the Pyrenees." *Tectonophysics* **129**: 173-203.
- Rahl, J. M., S. H. Haines and B. A. van der Pluijm (2011). "Links between orogenic wedge deformation and erosional exhumation: Evidence from illite age analysis of fault rock and detrital thermochronology of syn-tectonic conglomerates in the Spanish Pyrenees." *Earth and Planetary Science Letters* **307**(1-2): 180-190.
- Shuster, D. L. and K. A. Farley (2009). "The influence of artificial radiation damage and thermal annealing on helium diffusion kinetics in apatite." *Geochimica et cosmochimica acta* **73**(1): 183-196.
- Shuster, D. L., R. M. Flowers and K. A. Farley (2006). "The influence of natural radiation damage on helium diffusion kinetics in apatite." *Earth and Planetary Science Letters* **249**(3-4): 148-161.
- Sinclair, H. D., M. Gibson, M. Naylor and R. G. Morris (2005). "Asymmetric growth of the Pyrenees revealed through measurement and modeling of orogenic fluxes." *American Journal of Science* **305**: 369-406.
- Urgelés, R., A. Camerlenghi, D. Garcia-Castellanos, B. De Mol, M. Garcés, J. Vergés, I. Haslam and M. Hardman (2011). "New constraints on the Messinian sealevel drawdown from 3D seismic data of the Ebro Margin, western Mediterranean." *Basin Research* **23**(2): 123-145.
- Vergés, J., H. Millan, E. Roca, M. J. A., M. Marzo, J. Cites, T. Den Bezemer, R. Zoetemeijer and S. Cloetingh (1995). "Eastern Pyrenees and related foreland basins: pre-, syn- and post-collisional crustal-scale cross-sections." *Marine and Petroleum Geology* **12**(8): 893-915.
- Vergés, J. and J. A. Muñoz (1990). "Thrust sequences in the southern central Pyrenees." *Bulletin Société Géologique de France* **8**(2): 265-271.
- Vermeesch, P. (2009). "RadialPlotter: a Java application for fission track, luminescence and other radial plots." *Radiation Measurements* **44**(4): 409-410.
- Vincent, S. J. (2001). "The Sis palaeovalley: a record of proximal fluvial sedimentation and drainage basin development in response to Pyrenean mountain building." *Sedimentology* **48**(6): 1235-1276.
- Whitchurch, A. L., A. Carter, H. D. Sinclair, R. A. Duller, A. C. Whittaker and P. A. Allen (2011). "Sediment routing system evolution within a diachronously uplifting orogen: Insights from detrital zircon thermochronological analyses from the South-Central Pyrenees." *American Journal of Science* **311**(5): 442-482.
- Zeyen, H. and M. Fernández (1994). "Integrated lithospheric modeling combining thermal, gravity, and local isostasy analysis: Application to the NE Spanish Geotranssect." *Journal of Geophysical Research* **99**(B9): 18,089 - 18,102.

Sample	position (lat/long)	Elevation (m)	no of grains	$\rho_s$ (Ns) ( $10^6 \text{ cm}^{-2}$ )	$\rho_i$ (Ni) ( $10^6 \text{ cm}^{-2}$ )	$\rho_d$ (Nd) ( $10^6 \text{ cm}^{-2}$ )	$P\chi^2$ (%)	D	Central age ( $\pm 1\sigma$ , Ma)	MTL ( $\mu\text{m}$ )	sd ( $\mu\text{m}$ )	no tracks	Dpar ( $\mu\text{m}$ )	sd ( $\mu\text{m}$ )	no Dpar
AN01	41.96/00.85	624	8	1.133 (489)	0.632 (273)	0.74 (4262)	32.34	0.02	$144 \pm 11$	10.1	1.0	10	2.2	0.4	24
AN02	42.16/00.89	436	20	0.7641 (999)	0.8513 (1113)	0.75 (4262)	$\ll 1$	0.26	$76.9 \pm 6.2$	11.3	1.4	19	2.1	0.2	36
AN03	42.18/00.89	504	22	1.264 (1639)	1.493 (1936)	0.75 (4262)	$\ll 1$	0.26	$64.2 \pm 4.6$	12.2	1.6	27	2.2	0.2	61
AN04	42.22/00.84	902	13	1.0715 (810)	1.205 (911)	0.75 (4262)	$\ll 1$	0.20	$74.1 \pm 7.6$	11.3	2.2	19	2.1	0.1	18

700

701 **Table 1** Apatite Fission-Track results.  $\rho_s$  and  $\rho_i$  are the spontaneous and induced track densities measured;  $\rho_d$  is the induced track density in the external  
702 detector, the number of tracks counted (Ns, Ni, Nd) are in brackets;  $P(\chi^2)$  is  $\chi^2$ -probability (in %), D is the single-grain age dispersion. A  $P(\chi^2) < 5$  and/or  $D >$   
703 0.15 indicates that the data distribution contains multiple age populations ; MTL is the mean track length, with sd its standard deviation; Dpar is the average  
704 etch-pit width measured parallel to the C-axis. Measurements were performed by CF with a  $\zeta$ -factor =  $217.9 \pm 3.5$  for IRMM-540 dosimeter glasses.

705

706

707

708

709

710

711

712

Lab ID	Sample	$F_T$	Weight (ng)	Length/ Width/ Thickness ( $\mu\text{m}$ )	$^4\text{He} \times 10^{-6}$ (cc/g)	U (ppm)	Th (ppm)	Th/U	eU (ppm)	Age (Ma)	Age corr. $\pm 1\sigma$ (Ma)		
2486	AN011	0.76	2.9	128	101	95	122	12.9	19.2	1.5	17.5	58.0	<b><math>76.9 \pm 7.1</math></b>
2488	AN012	0.80	5.7	181	123	108	4.1	2.8	6.3	2.3	4.3	5.2	<b><math>6.5 \pm 0.6</math></b>
2493	AN022	0.76	3.4	146	106	92	9.4	9.9	11	1.1	12.5	6.2	<b><math>8.1 \pm 0.7</math></b>
2495	AN023	0.84	6.7	156	139	132	5.4	5.8	33.6	5.8	13.9	3.2	<b><math>3.9 \pm 0.3</math></b>
2499	AN031	0.76	3.9	187	100	85	48.5	9.8	39.6	4	19.3	20.9	<b><math>27.6 \pm 2.5</math></b>
2501	AN032	0.87	5.3	177	135	117	117	22.3	20.5	0.9	27.2	35.7	<b><math>41.0 \pm 3.8</math></b>
2548	AN033	0.69	10	151	77	67	120	12	54.9	4.6	25.2	39.6	<b><math>57.4 \pm 5.3</math></b>
1641	AN034	0.84	11.5	200	150	187	20.6	15.9	8.9	0.56	18	9.5	<b><math>11.3 \pm 1.0</math></b>
1643	AN035	0.80	5	150	125	112	6.2	4	14.2	3.55	7.4	6.9	<b><math>8.7 \pm 0.8</math></b>
2552	AN051	0.80	4.6	190	113	97	326	49.2	616.3	12.5	197.1	13.8	<b><math>17.2 \pm 1.6</math></b>
2554	AN052	0.80	5	147	120	112	224	27.9	362.4	13	114.9	16.3	<b><math>20.3 \pm 1.9</math></b>
1878	AN053	0.85	12.6	275	175	125	53.2	6.4	29.9	4.67	13.6	32.6	<b><math>38.5 \pm 3.5</math></b>
1880	AN054	0.80	12.8	262	162	162	335	10.6	36.5	3.43	19.4	144.0	<b><math>169.1 \pm 15.6</math></b>

713

714 **Table 2.** Apatite (U-Th)/He results. Lab ID is the Orsay sample identification number, which is the second replicate  $^3\text{He}$  spike pipette number,  $F_T$  is the  
715 geometric correction factor for age calculation; age corr. is the age corrected by the ejection factor  $F_T$ , the uncertainty  $1\sigma$  was fixed at 8 % of the age. eU is  
716 the effective uranium concentration.

## Figure captions

**Figure 1.** a) Regional map of the Pyrenean range and its two foreland basins, the black box represents the study area shown in map b. NPZ: North Pyrenean Zone; SCU: South Central Unit. b) Simplified geological map of the southern central Pyrenees (modified from ICC 2002), with sample positions and location of cross-section shown in c. c) Geological cross-section drawn from the ECORS seismic profile (Muñoz 1992); sample positions have been projected on the section.

**Figure 2.** Radial-plot and histogram representations (Vermeesch 2009) of the AFT counting data of samples AN01, 02, 03, and 04 combined. The radial plot is centred on the central age of the combined samples (79 Ma); grey lines indicate peak ages and the black dashed line represents the depositional age (65 Ma). Samples are individualised by different grey-shading of the data points.

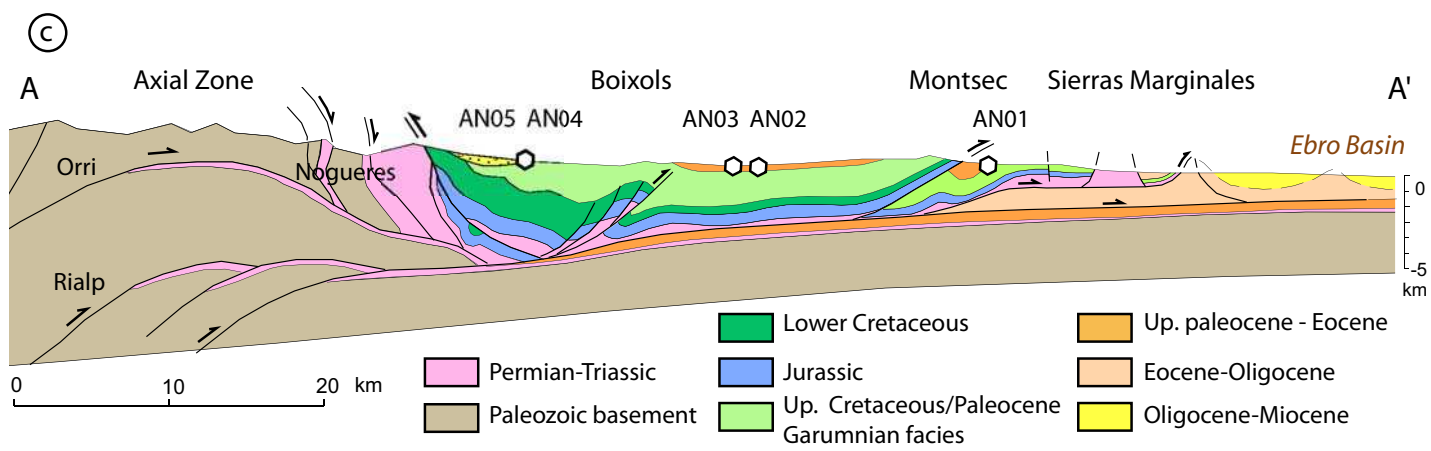
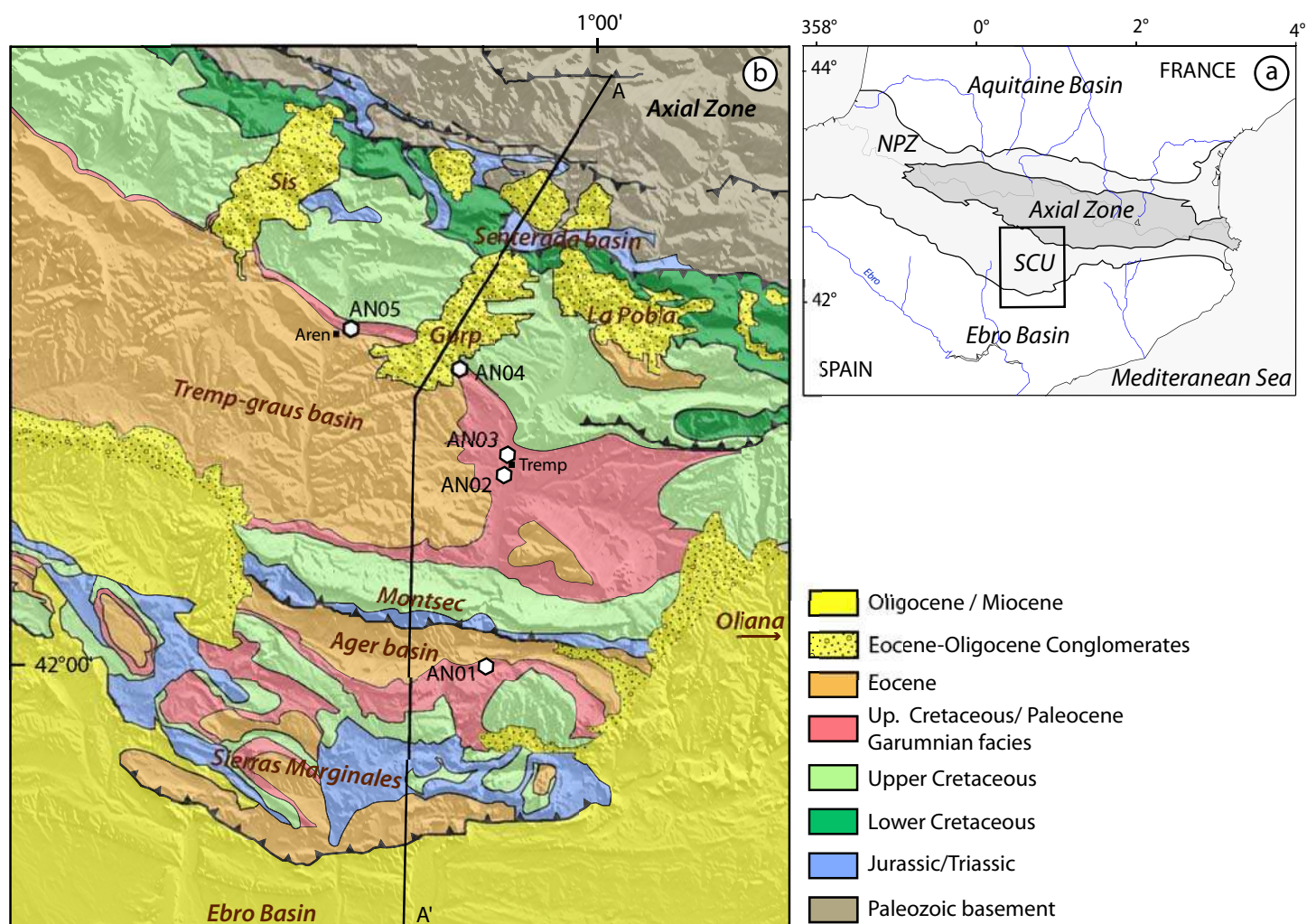
**Figure 3.** a) AHe ages plotted as a function of effective uranium content ( $eU = [U] + 0.24 \times [Th]$ ) for the four samples analysed; gray dashed line in a) represents exponential fit to the data. b) Sample AN05 has been separated from the others due to its high eU content and lack of correlation between eU and AHe ages, which contrasts with the other samples.

**Figure 4.** Modelled  $T-t$  paths from joint AFT and AHe data for samples AN01, 02 and 03 (note variable timescales for these plots, constrained by the oldest single-grain AFT age). The black curves represent the expected model (weighted mean model) and its 95% confidence interval for the  $T-t$  paths; the yellow curve is the maximum likelihood model (best data fit).  $T-t$  paths are coloured according to their probability (scale on the right-hand side, which varies between samples). The gray boxes represent the prior constraints on the explored parameter space (see text for discussion) and dotted gray lines refer to the values of  $T_{max}$  and burial time discussed in the text.

**Figure 5.** Sensitivity of AHe ages to eU variations. The curves represent predicted AHe ages as a function of eU for the  $T-t$  paths of the expected models (cf. Fig. 4), and for eU varying from 5 to 30 ppm. The dots represent the AHe data shown in Fig. 3 and Table 2.

**Figure 6.** Effect of pre-depositional exhumation history on AHe ages. a) Forward model set up: AHe ages are predicted using the He-diffusion model of Flowers *et al.* (2009) for varying eU contents,  $T_{max}$  and starting times of pre-depositional exhumation (“exhumation 1”). b) AHe ages modelled as a function of eU content and starting time of the pre-depositional phase of exhumation, for two different maximum burial temperatures ( $T_{max} = 70$  and  $80$  °C respectively). Measured ages of our samples are plotted as black squares, or represented as dashed lines when they do not resolve a starting time.

**Figure 7.** Topographic profile along the same transect as A-A' in Figure 1b, showing the inferred palaeo-elevation of the Oligocene-Miocene deposits inferred from thermal-history modelling of the AHe and AFT data for samples AN02, AN03 and AN01 (dashed line is best estimate, orange band is uncertainty), compared to the inferred maximum elevation over the southern Axial Zone from inversion of *in-situ* thermochronology data (Fillon & van der Beek 2012). Yellow shading in Sierra de Gulp represents current exposure of Late Eocene–Oligocene conglomerates. Locations of major thrust faults in the SCU fold-and-thrust belt are indicated for comparison to Fig. 1c.





# AN01, AN02, AN03 and AN04 combined

Central age = 79,3 +/- 7,9 Ma (2se)

Peak 1: 51,8 +/- 3,2 Ma

Peak 2: 76,2 +/- 3,7 Ma

Peak 3: 142 +/- 10 Ma

